



# Effect of expandable and expanded graphites on the thermo-mechanical properties of polyamide I I

Journal of Elastomers &amp; Plastics

2019, Vol. 51 (2) 175–190

© The Author(s) 2018

Article reuse guidelines:

[sagepub.com/journals-permissions](https://sagepub.com/journals-permissions)

DOI: 10.1177/0095244318781956

[journals.sagepub.com/home/jep](https://journals.sagepub.com/home/jep)

F Oulmou<sup>1</sup>, A Benhamida<sup>1</sup>, A Dorigato<sup>2</sup>, A Sola<sup>3</sup> ,  
M Messori<sup>3</sup> and A Pegoretti<sup>2</sup>

## Abstract

The preparation and thermo-mechanical characterization of composites based on polyamide I I (PAI I) filled with various amounts of both expandable and expanded graphites are presented. Investigation conducted using X-ray diffraction (XRD), scanning electron microscopy and surface area analyses indicated how graphite expanded under the selected processing conditions. The XRD analysis on PAI I/graphite composites revealed no change in the crystal form of the PAI I, while the presence of diffraction peaks associated to the graphite-stacked lamellae can be still detected. All the investigated composites showed an improvement of the thermal stability and mechanical properties (elastic and storage moduli).

## Keywords

Polyamide, expandable graphite, expanded graphite, thermal properties, mechanical properties

## Introduction

Polyamides are thermoplastic polymers that exhibit high strength, abrasion resistance, stiffness and stability of their physical and mechanical properties over a wide range of temperatures. The semicrystalline structure and the intermolecular hydrogen bonds of the amide groups are responsible for the advantageous properties of the polyamides.<sup>1</sup>

<sup>1</sup> Laboratoire des Matériaux Polymères Avancés (LMPA), Université Abderrahmane Mira de Bejaia, Bejaia, Algeria

<sup>2</sup> Department of Industrial Engineering, University of Trento, Trento, Italy

<sup>3</sup> Department of Engineering 'Enzo Ferrari', University of Modena and Reggio Emilia, Modena, Italy

## Corresponding author:

A Dorigato, Department of Industrial Engineering, University of Trento, Via Sommarive 9, 38123 Trento, Italy.

Email: [andrea.dorigato@unitn.it](mailto:andrea.dorigato@unitn.it)

They are used in various fields, ranging from household devices, clothing, carpets and stockings, to more technical products such as pipelines, tubes, gears and automotive components.<sup>2–6</sup>

Polyamide 11 (PA11) is one of the most promising engineering plastics for several reasons, one of which is that it derives from a renewable resource such as the castor oil. In addition, it can be used in a large number of applications thanks to its outstanding properties such as excellent resistance to chemicals (particularly hydrocarbons), high impact strength, ease of processing, wide range of service temperatures ( $-40^{\circ}\text{C}/+130^{\circ}\text{C}$ ), high dimensional stability and low density. PA11 is widely used in industrial areas from automotive to offshore oilfield applications, and many efforts have been made to improve its mechanical performance as well as its ferroelectric and piezoelectric property and to reduce its yield cost.<sup>7–9</sup>

Polymer nanocomposites attracted a great deal of attention and have been the focus of study for a large number of research groups.<sup>10–14</sup> In recent years, polymer-based nanocomposites reinforced with expandable graphite have received much attention by both scientific and industrial communities due to their enhanced mechanical performances, electrical conductivity and barrier properties as well as flame resistance over neat polymers.<sup>15</sup> The reasons for the observed behaviour depend on the structure of natural graphite where the atoms in a plane are strongly bonded in an hexagonal structure but weakly bonded normal to that plane. These sheets/layers can be exfoliated to high aspect ratio (200–1500) graphite nanosheets with elevated in-plane modulus (approximately 1 TPa).<sup>16</sup> Furthermore, graphite nanosheets have an enormous surface area (up to  $2600\text{ m}^2\text{ g}^{-1}$ ), considering that both sides of the sheets are accessible.<sup>15</sup> Therefore, a good dispersion of such nanosheets in a matrix can play a key role in the improvement of both physical and mechanical properties of the resulting composites.<sup>17</sup>

Expandable graphite (NEG) is a partially oxidized form of graphite containing intercalated guest species (e.g. sulfuric acid anions) in between the stacked graphene layers.<sup>18,19</sup> Industrial-scale synthesis of expandable graphite can be performed via liquid-phase graphite–sulfuric acid reactions in the presence of strong chemical oxidants such as potassium permanganate, nitric acid and hydrogen peroxide.<sup>20,21</sup> A key property of expandable graphite is its tendency to exfoliate when it is exposed to high temperatures. According to Chung,<sup>22</sup> the origin of this process lies in the vaporization of the intercalated guest ions, forming a gas that causes the flakes to rapidly expand in a worm-like manner and to occupy a larger volume. This implies that the gases that cause the expansion of the expandable graphite mainly contain carbon dioxide and sulphur dioxide.<sup>23</sup>

A number of studies have been conducted on polymer-based nanocomposites reinforced with expanded graphite, and these studies have shown substantial improvements in mechanical behaviour, electrical conductivity and barrier properties as well as flame resistance in several polymers. Uhl et al.<sup>24</sup> studied the mechanical and fire-retardant properties of polyamide-6/expandable graphite nanocomposites. When they compared them to PA6/montmorillonite clay nanocomposites with similar filler dispersion, the PA6/expandable graphite nanocomposites showed higher improvements in flame-retardant

properties but not as good thermo-mechanical properties as the corresponding PA6/clay nanocomposites. Fukushima et al.<sup>17</sup> reported that polylactic acid (PLA) nanocomposites with expanded graphite showed considerable improvements in the thermal, mechanical and fire-retardant properties with respect to the original PLA. Li and Qu<sup>25</sup> studied the synergistic effects on the flammability behaviour provided by different types of expandable graphite with magnesium hydroxide in halogen-free flame-retardant/ethylene vinyl acetate blends. A consistent improvement in flame-retardant properties was detected through cone calorimetry tests. Wei et al.<sup>26</sup> used expandable graphite to develop fire-retardant biobased polylactide composites. Thermal stability and flammability properties were assessed through thermogravimetric analysis (TGA), cone calorimeter measurements and UL94 tests. Forced combustion tests indicated that the rate of combustion was sensibly decreased because of the protective intumescent char formed on the surface of the material at elevated graphite contents.

To the best of our knowledge, however, no studies have been so far reported on the effect of expandable graphite in PA11. Therefore, in this article a comprehensive study of the microstructural, thermal and mechanical properties of PA11/graphite nanocomposites prepared by melt blending is reported. Particular attention was devoted on how graphite with different treatments could affect the physical properties of the resulting materials.

## Experiment

### Materials

PA11 chips (Rilsan<sup>®</sup> BESNO TL NB), with a density of  $1.02 \text{ g cm}^{-3}$  and a melting temperature ( $T_m$ ) of  $186^\circ\text{C}$ , were supplied by Arkema Specialty Polyamides (Colombes Cedex, France). Rilsan PA11 is a high-performance polymer fully obtained from renewable resources (i.e. castor oil). The selected grade does not contain additives. Expandable graphite (NEG) grade ES250 B5 (nominal onset expansion temperature  $220^\circ\text{C}$ ) was purchased from Qingdao Kropfmuehl Graphite (China). In the producer's datasheet, a mean particle width of about  $300 \mu\text{m}$  is reported. According to the indications reported in the article of Focke et al.,<sup>11,27</sup> expanded graphite (EG) was prepared by treating NEG powder at high temperature for 5 min, by placing it in a muffle furnace set at  $700^\circ\text{C}$ , at atmospheric pressure.

### Preparation of PA11 nanocomposite samples

Before processing, PA11 was dried at  $80^\circ\text{C}$  in a vacuum oven for 24 h, in order to eliminate the moisture and to reduce the degradation of the polymer matrix during the melt processing. Both expandable graphite (NEG) and expanded graphite (EG) were considered as fillers. The PA11/graphite nanocomposites were prepared by melt compounding in a Haake PolyLab Rheomix 600 mixer (Karlsruhe, Germany) at a temperature of  $225^\circ\text{C}$ , with a residence time of 5 min and a rotation speed of  $60 \text{ r min}^{-1}$ . The filler content was varied from 1 wt% to 10 wt%. The compounded materials were then compression molded using a Carver laboratory press (Wabash, Indiana, USA) at  $225^\circ\text{C}$  for 5 min. In this way, square sheets about 1 mm thick were obtained.

### Experimental techniques

**X-ray diffraction.** X-ray diffraction (XRD) was performed on expandable graphite (NEG), expanded graphite (EG) and the compression-molded nanocomposite sheets in order to evaluate the crystalline structure of the PA11 matrix and the degree of expansion/exfoliation of graphite nanoplatelets in the nanocomposites. XRD measurements were carried out on a X'pert PROPANalytical analyzer, using copper  $K_\alpha$  radiation ( $\lambda = 1.54 \text{ \AA}$ ), a generator tension of 40 kV and a current of 40 mA. Scans were taken in a  $2\theta$  interval between  $5^\circ$  and  $60^\circ$ , with a  $2\theta$  step of  $0.016^\circ$ .

**Scanning electron microscopy.** The morphology of the prepared composites was investigated with a Zeiss AG Supra 40 field-emission scanning electron microscope (FESEM) operating in a high vacuum mode. The samples were cryogenically fractured in liquid nitrogen and then a platinum–palladium sputtering was performed on their surfaces.

**Specific surface area.** The specific surface areas of the graphite powders were determined according to the Brunauer–Emmett–Teller (BET) theory using a Micromeritics Instrument (Norcross, GA, USA) and a Nova 1000e BET instrument (Boynton Beach, FL, USA) under nitrogen atmosphere at 77 K.

**Thermogravimetric analysis.** TGAs were performed through a TGAQ500 machine, provided by TA Instruments (New Castle, DE, USA). Samples with a mass of approximately 15 mg were placed in open alumina pans and heated from  $50^\circ\text{C}$  to  $700^\circ\text{C}$  at a heating rate of  $10^\circ\text{C}\cdot\text{min}^{-1}$  under a constant nitrogen flow of  $10 \text{ ml min}^{-1}$ . In this way, it was possible to evaluate the thermal stability of the PA11 nanocomposites by measuring the temperature associated to a mass loss of 5% ( $T_{5\%}$ ), the temperature of maximum degradation rate ( $T_d$ ) and the char yield at  $700^\circ\text{C}$  ( $m_{700}$ ).

**Differential scanning calorimetry.** The crystallinity and the thermal transition temperatures of the nanocomposite samples were evaluated through a Mettler® DSC 30 (Schwerzenbach, Switzerland) apparatus under nitrogen flow of  $100 \text{ ml min}^{-1}$ . After a first heating run from  $0^\circ\text{C}$  to  $250^\circ\text{C}$  at  $10^\circ\text{C min}^{-1}$ , a cooling step down to  $0^\circ\text{C}$  and a second heating run were performed at the same rate. The crystallization temperature ( $T_c$ ) was obtained from the cooling scan; the glass transition temperature ( $T_g$ ), the  $T_m$  and the melting enthalpy ( $\Delta H_m$ ) were determined from the second heating scan. The degree of crystallinity ( $X_c$ ) of the PA11 matrix was calculated using equation (1):

$$X_c = \frac{\Delta H_m}{\Delta H_0 \times W_t} \times 100 \quad (1)$$

where  $\Delta H_0$  is the melting enthalpy of 100% crystalline polymer (i.e.  $206 \text{ J}\cdot\text{g}^{-1}$  from<sup>28</sup>) and  $W_t$  is the PA11 weight fraction in the composites.

**Dynamic mechanical analysis.** Dynamic mechanical analysis (DMA) was performed using a DMA Q800 testing machine (New Castle, DE, USA). Rectangular specimens 15 mm

long, 5 mm wide and 1 mm thick were tested. The data were collected after heating the samples from 0°C to 150°C at a heating rate of 3°C min<sup>-1</sup>, with a frequency of 1 Hz. The thermo-mechanical behaviour of the nanocomposite samples was thus investigated, and the trends of the storage modulus ( $E'$ ) and of the damping factor ( $\tan \delta$ ) as a function of the testing temperature were registered. The  $T_g$  was evaluated as the temperature associated to the damping factor peak.

**Quasi-static tensile tests.** Uniaxial quasi-static tensile tests were carried out at a temperature of 23°C and a relative humidity of 50%, using an Instron<sup>®</sup> 5969 tensile testing machine (Norwood, Massachusetts, USA). ISO 527 1 BA-type dumb-bell specimens with a gauge length of 30 mm were punched out from the prepared sheets. Elastic modulus was evaluated at a crosshead speed of 0.25 mm min<sup>-1</sup> using an Instron 2620-601 resistance extensometer, having a gauge length of 12.5 mm, considering a secant stress value between deformation levels of 0.05% and 0.25%. Tensile tests at break were carried out at a crosshead speed of 50 mm min<sup>-1</sup> without using the extensometer, and deformation was estimated by normalizing the crosshead displacement over the initial gauge length of the specimens (30 mm). At least five specimens were tested for each sample.

## Results and discussion

### *Structural behaviour of graphite-based nanofillers*

Figure 1 shows XRD diffractograms for the expandable graphite (NEG) and expanded graphite (EG) powders. Both diffractograms show a peak at  $2\theta = 26.16^\circ$  corresponding to a d-spacing of 0.340 nm that can be attributed to the intercalation of sulfuric acid.<sup>20,29</sup> It is clear from these diffractograms that the NEG is mainly composed of single intercalated structures, but it also shows the coexistence of non-intercalated and intercalated layers of sulfuric acid (i.e. the flakes also contain non-intercalated graphite layers). After the expansion, there is a reduction of the intensity of the peak at  $2\theta = 26.16^\circ$ , attributed to decomposition of the sulfuric acid, leading to a lower amount of intercalated graphitic structures. The reported results find confirmation in some literature studies on the morphology of expandable graphite flakes before (NEG) and after (EG) expansion process.<sup>20,30</sup>

Figure 2 shows the FESEM micrographs of graphite samples. The microstructure observed for the EG sample, obtained after the heat treatment of the expandable graphite flake at 700°C, exhibits a worm-like or accordion-like structure composed of multiple nano-scaled platelets joint together. The NEG platelets were expanded during high-temperature treatment, thus reaching a thickness a few hundred times higher than the initial value (around 12  $\mu\text{m}$ ), while their diameter remained almost unchanged, as already reported by Fock et al.<sup>23</sup> The accordion-like microstructure of the expanded EG worms is built up of distorted graphite sheets. Because of their very high aspect ratio, the average thickness of these sheets can be estimated from the BET surface area using equation (2):

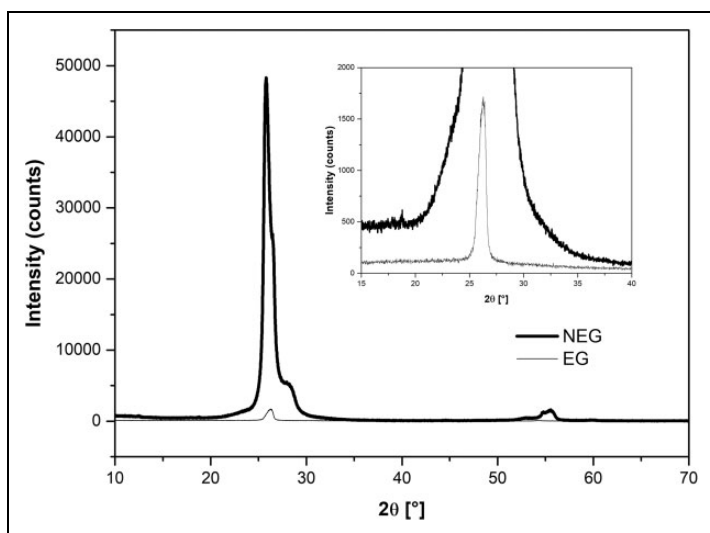


**Figure 1.** XRD patterns of expandable graphite (NEG) and expanded graphite (EG) nanofillers. XRD: X-ray diffraction.

$$t = \frac{2}{\rho A} \quad (2)$$

where  $t$  is the average sheet thickness in m,  $\rho$  is the density in  $\text{kg m}^{-3}$  and  $A$  is the BET surface area in  $\text{m}^2 \text{g}^{-1}$ . It is important to underline that equation (2) neglects the edge surface area of the flakes. The value of the BET surface area of NEG ( $0.9582 \pm 0.0126 \text{ m}^2 \text{g}^{-1}$ ) is increased up to  $23.5076 \pm 0.6619 \text{ m}^2 \text{g}^{-1}$  after thermal treatment. Applying equation (2) to the EG sample, an average flake thickness of about 38 nm can be determined. The same value was found in the literature,<sup>20</sup> and the nanostructured nature of the expanded ‘worms’ is therefore confirmed. By comparing the results obtained from XRD, FESEM and BET with those present in the literature,<sup>15,23,27,29,31</sup> it can be concluded that the preparation of the expanded graphite (EG) filler was successfully performed.

### Morphology of PA11/graphite nanocomposites

In order to investigate the influence of the different typologies of graphite on the crystalline structure of PA11 and to study the dispersion of these nanofillers within the PA11 matrix, XRD and FESEM analyses were conducted. Figure 3 shows XRD patterns of PA11/NEG and PA11/EG nanocomposites with different filler contents, and the XRD pattern of neat PA11 is also shown for comparison. The d-spacing determined by applying the Bragg’s law starting from the position of the main reflections detected in the diffractograms is reported in Table 1.

The main crystalline peaks in the XRD patterns of the neat PA11 can be observed at  $2\theta = 7.23^\circ$ ,  $20.23^\circ$  and  $22.90^\circ$ . According to Liu et al.<sup>32</sup>, these reflections correspond to

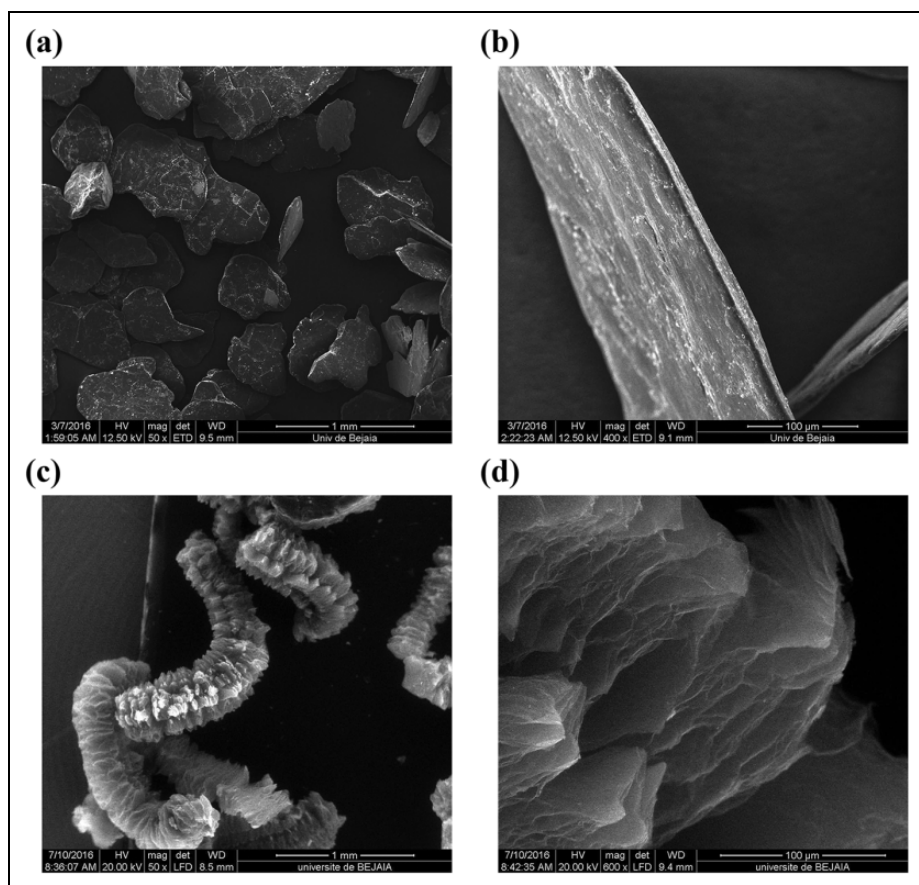


**Figure 2.** FESEM micrographs of graphite samples: (a) NEG powder at low resolution and (b) at high resolution, (c) EG powder at low resolution and (d) at high resolution. FESEM: field-emission scanning electron microscope.

(001), (100) and (010/110) planes of the  $\alpha$  polymorph of nylon 11, respectively. It is worth noting that the neat PA11 does not show any peak at  $26.16^\circ$ , while PA11/NEG and PA11/EG composites show characteristic diffraction peaks at  $2\theta = 26.16^\circ$ . This angular position can be utilized to determine the d-spacing of NEG and EG fillers in the composites. It can be noticed that the intensity of this peak also strongly increases as the fillers content increases, but its position does not change. This means that the structure of graphite does not substantially change when it is compounded with PA11, in contrast to the results reported by Uhl et al.<sup>24</sup> on PA6/expandable graphite composites. Considering that the d-spacing reflects the extent of nanofiller dispersion during the composite formation, it can be supposed that a relatively low filler dispersion in the PA11 matrix was achieved. In other words, the appearance of this sharp peak suggests that not all the graphite galleries were expanded and subsequently not all graphite was dispersed as

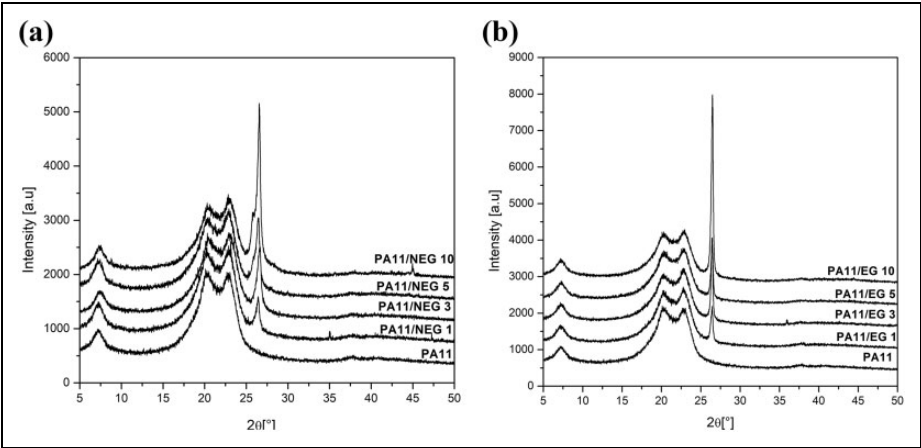


**Figure 3.** XRD patterns of (a) neat PA11 and PA11/NEG nanocomposites and (b) neat PA11 and PA11/EG nanocomposites. XRD: X-ray diffraction.

**Table 1.** Results obtained from XRD analysis on PA11-based nanocomposites.

Sample	2θ peak (°)	d-Spacing (nm)
PA11/NEG 1	26.38	0.337
PA11/NEG 3	26.60	0.335
PA11/NEG 5	26.43	0.337
PA11/NEG 10	26.55	0.335
PA11/EG 1	26.38	0.337
PA11/EG 3	26.40	0.337
PA11/EG 5	26.41	0.337
PA11/EG 10	26.42	0.337

XRD: X-ray diffraction; PA11: polyamide 11.

layers in PA11. Thus, the XRD results indicate that all the investigated composites in this study include some non-dispersed graphite layers, probably originating from non-expanded graphite clusters. It can be also noticed that the crystalline structure of PA11 is practically not affected by the presence of graphite filler in the composites, and PA11 still crystallizes in a stable triclinic  $\alpha$ -form.

Figure 4 shows FESEM images of the cryofractured surfaces of PA11/NEG and PA11/EG composites, taken at various magnifications. In Figure 4(a) and (b), sheet-like NEG stacks with different size can be clearly seen in the composite structure. It can be concluded that NEG flakes exhibit a relatively poor dispersion into the PA11 matrix, with a rather limited interfacial interaction between the filler and the polymer phase. The low dispersion of the NEG through the PA11 matrix can be due to the method of incorporation of the NEG during the preparation of the composite. If the PA11/EG composites are considered (see



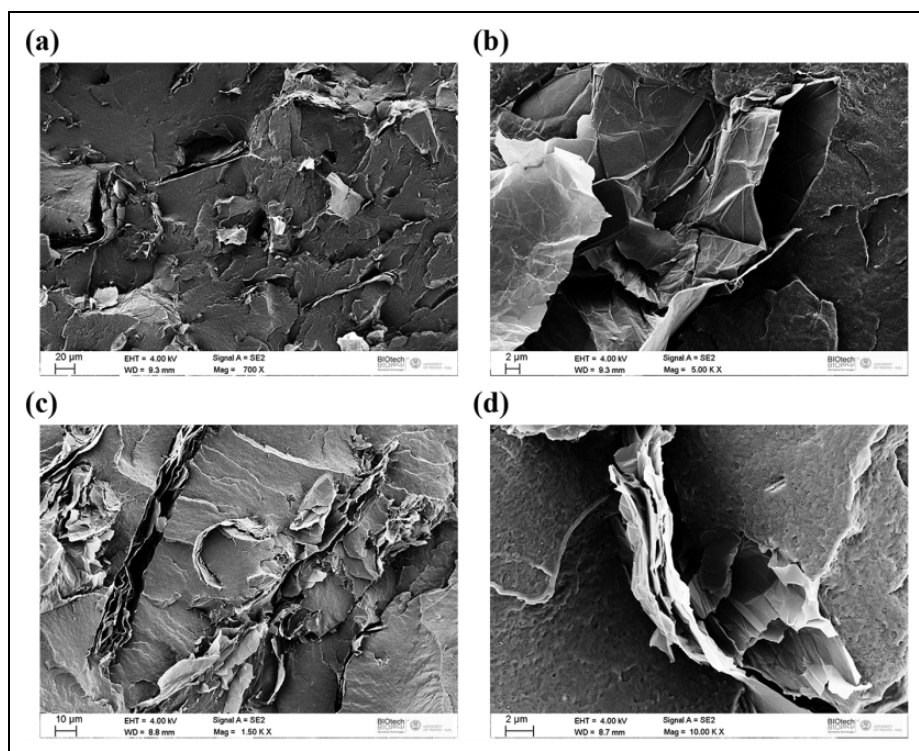


**Figure 4.** FESEM images of the fractured surfaces of (a and b) PA11/NEG and (c and d) PA11/EG nanocomposites at different magnifications. FESEM: field-emission scanning electron microscope.

Figure 4(c) and (d)), stacked sheets of EG are also observed in the composite structure. Based on the scanning electron microscope images, it can be concluded that also EG-loaded samples exhibit a relatively low nanosheets dispersion into the PA11 phase.

### Thermal behaviour

In order to explore further thermal decomposition behaviour of the prepared composites, TGA of PA11/NEG and PA11/EG composites was performed under inert ( $N_2$ ) atmosphere. In Table 2, the results of TGA tests, expressed in terms of  $T_{5\%}$ ,  $T_d$  and  $m_{700}$ , are reported. Considering  $T_{5\%}$  values, it seems that the onset degradation temperature is not substantially affected by the presence of NEG, and a small  $T_{5\%}$  decrease (about  $5^\circ C$ ) can be detected. According to some authors,<sup>12,13,33</sup> this decrease may be attributed to the presence of the sulfuric acid within the expandable graphite sheets, thus the release of acid degradation products can facilitate degradation of the PA11 at lower temperatures. On the other hand, a slight  $T_{5\%}$  increase can be seen in the case of EG filler composites. The same trend can be detected if degradation temperature values ( $T_d$ ) are considered. This behaviour could be probably explained considering the better exfoliation of

**Table 2.** Results of TGA tests on PA11/EG and PA11/NEG nanocomposites.

Sample	$T_{5\%}$ ( $^{\circ}\text{C}$ )	$T_d$ ( $^{\circ}\text{C}$ )	$m_{700}$ (%)
PA11	400.2	453.3	0.3
PA11/NEG 1	395.7	439.7	1.2
PA11/NEG 3	391.9	457.6	2.6
PA11/NEG 5	393.9	453.3	4.3
PA11/NEG 10	393.2	458.0	6.2
PA11/EG 1	399.4	446.3	1.1
PA11/EG 3	401.9	452.3	3.5
PA11/EG 5	403.5	460.0	5.1
PA11/EG 10	407.7	463.3	9.4

TGA: thermogravimetric analysis; PA11: polyamide 11;  $T_{5\%}$ : temperature associated to a mass loss of 5%;  $T_d$ : temperature of maximum degradation rate;  $m_{700}$ : the char yield at 700 $^{\circ}\text{C}$ .

graphite nanoplatelets due to the thermal expansion process. It is also interesting that the char yield is proportional to the percentage of filler contents, except for the highest loading (PA11/NEG 10) where a  $m_{700}$  of 6.2%, instead of a value close to 10%, was found. Therefore, it can be concluded that the thermal stability of PA11 is enhanced by the presence of expanded graphite, while NEG introduction does not improve the thermal degradation resistance of the material.

In order to analyse the influence of the graphite fillers on the melting behaviour and on the crystallinity of the PA11 matrix, DSC tests were conducted. In Figure 5(a) and (d), DSC thermograms of neat PA11 and of the relative composites at different concentrations are represented, while the most important results are summarized in Table 3. It is evident that the thermal transitions of the material are practically not affected by the presence of the fillers, and both  $T_m$  and  $T_g$  of the PA11/NEG and PA11/EG composites are practically the same of the neat PA11. However, a slight increase in the crystallization temperature ( $T_c$ ) (+4 $^{\circ}\text{C}$  for an NEG amount of 10 wt%) and in the crystallinity degree of PA11 (+5% for an NEG concentration of 10 wt%) can be detected with the NEG loading. This increase in the crystallization temperature, though not so pronounced, can be attributed to the heterogeneous nucleation effects of polymer matrices in the presence of nanoparticles.<sup>28</sup> In the case of the PA11/EG composites, the effect of the nanofiller on the crystallization temperatures and on the crystallinity degree is rather limited, even at elevated EG loading.

### Dynamic mechanical properties

The trends of the storage modulus ( $E'$ ) and of the loss tangent ( $\tan \delta$ ) of PA11/NEG and PA11/EG composites from 0 $^{\circ}\text{C}$  to 150 $^{\circ}\text{C}$  are shown in Figures 6 and 7, respectively. The storage modulus values ( $E'$ ) for the PA11/NEG and PA11/EG composites are higher than that of the neat PA11.  $E'$  exhibits an increase with the addition of filler contents for both NEG and EG systems. However, the increase in EG composites (about 31% with an EG loading of 10 wt%) is more intense than that observed for NEG-filled systems at the

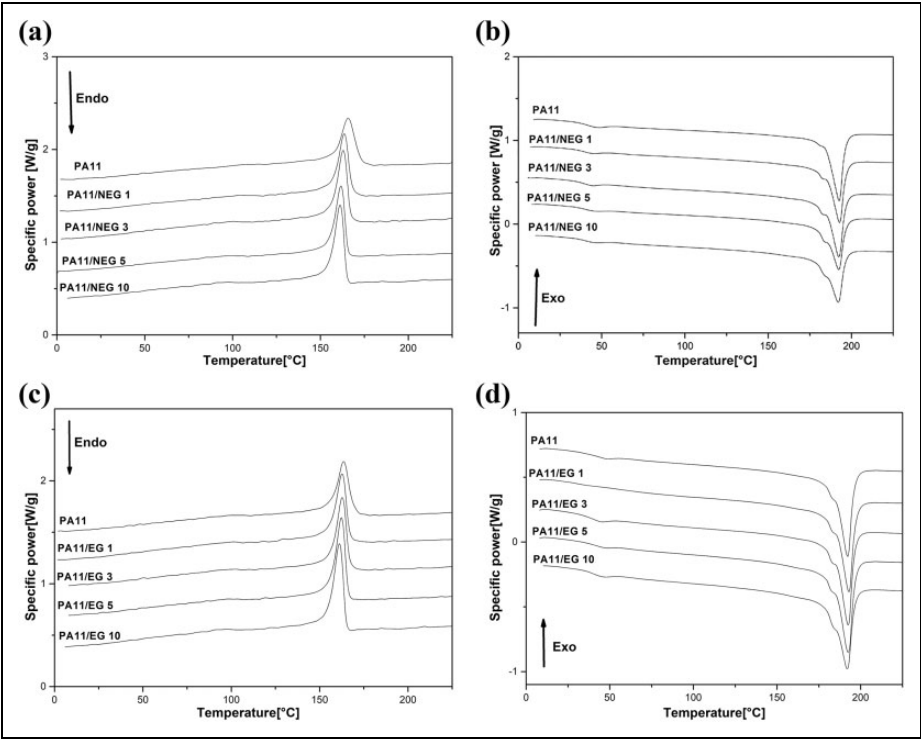


**Figure 5.** DSC thermograms of (a) PA11 and PA11/NEG samples (cooling stage), (b) PA11 and PA11/NEG samples (heating stage), (c) PA11 and PA11/EG samples (cooling stage) and (d) PA11 and PA11/EG samples (heating stage).

**Table 3.** Results of DSC tests on neat PA11 and on the relative nanocomposites.

Samples	$T_g$ (°C)	$T_m$ (°C)	$T_c$ (°C)	$X_c$ (%)
PA11	40.9	187.2	163.2	22.5
PA11/NEG 1	39.5	187.2	163.4	22.8
PA11/NEG 3	39.0	187.8	164.6	27.2
PA11/NEG 5	39.5	188.5	165.2	24.3
PA11/NEG 10	40.1	188.8	167.2	25.8
PA11/EG 1	42.0	187.6	164.2	24.4
PA11/EG 3	39.7	187.1	164.4	23.9
PA11/EG 5	43.1	187.4	164.4	23.5
PA11/EG 10	42.8	187.3	165.4	24.1

PA11: polyamide 11;  $T_g$ : glass transition temperature;  $T_m$ : melting temperature;  $T_c$ : crystallization temperature;  $X_c$ : degree of crystallinity.

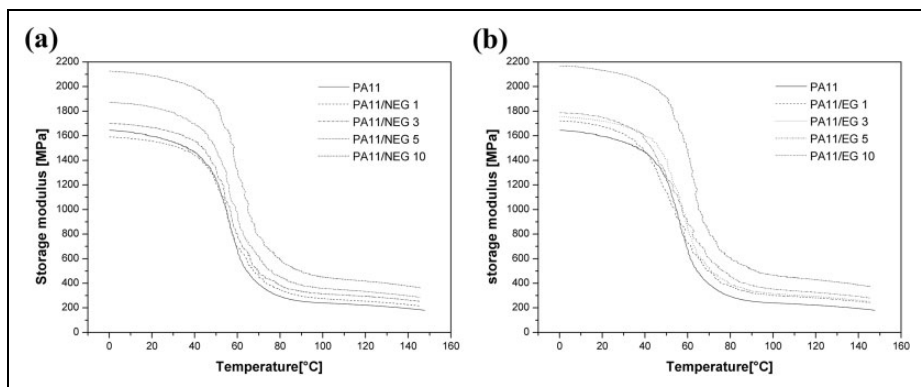


**Figure 6.** Storage modulus ( $E'$ ) from DMA tests of (a) PA11/NEG and (b) PA11/EG composites. DMA: dynamic mechanical analysis.

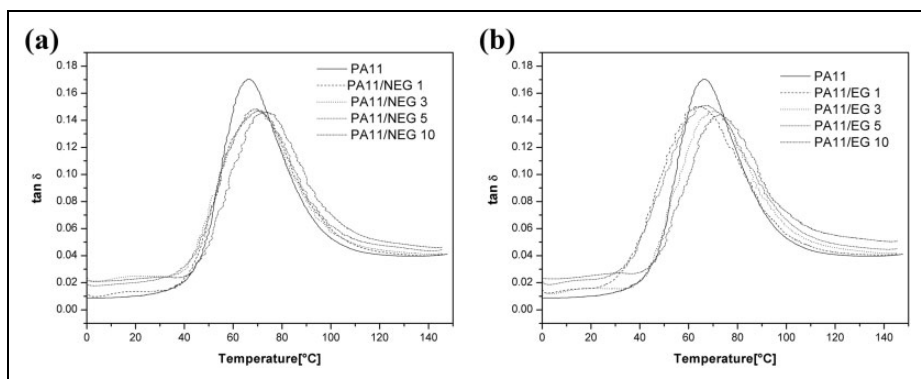


**Figure 7.** Loss tangent ( $\tan \delta$ ) values from DMA tests of (a) PA11/NEG and (b) PA11/EG nanocomposites.

same filler loading. The observed improvement in storage modulus of PA11/graphite composites could be probably attributed to the stiffening effect provided by the nano-filler, especially at elevated concentrations. Another interesting feature is that the  $T_g$  values detected through DMA analysis are considerably higher than those revealed by DSC tests. As already reported in the literature, the  $T_g$  values found in DSC tests are usually 10–20°C lower than those evaluated in DMA. This is probably due to the following reasons: (i) the maximum of the  $\tan \delta$  curve (usually considered as the  $T_g$  of the materials) is the centre of the relaxation, whereas in the DSC experiment the onset temperature of the  $T_g$  relaxation is usually reported<sup>32</sup>; (ii) a different heating rate was utilized in the tests (3°C min<sup>-1</sup> for DMA and 10°C·min<sup>-1</sup> in DSC measurements). Another interesting feature from DMA is that the  $T_g$  does not substantially change with the filler amount.

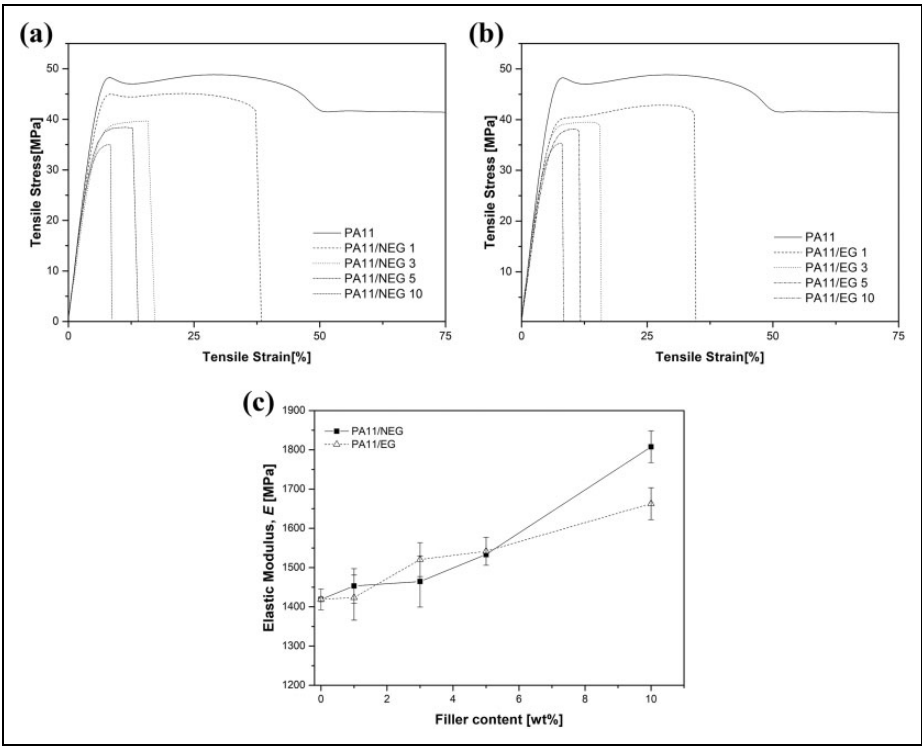


**Figure 8.** (a) Stress–strain curves of neat PA11 and PA11/NEG nanocomposites, (b) stress–strain curves of neat PA11 and PA11/EG nanocomposites and (c) tensile modulus of neat PA11 and relative nanocomposites.

*Tensile properties*

Representative stress–strain curves of the neat PA11 and the relative composites are shown in Figure 8(a) and (b), while the trends of the tensile modulus as a function of the nanofiller amount are reported in Figure 8(c). Even if all the composites show a higher modulus with respect to the neat PA11 (+27% with an NEG content of 10 wt% and +17% with an EG amount of 10 wt%), a heavy reduction of the ultimate properties can be detected, especially at elevated filler amounts. A similar behaviour was also observed for graphite-reinforced epoxy composites.<sup>15</sup> It can be therefore concluded that the prepared composites are stiffer and more brittle in comparison with neat PA11, irrespective of the graphite expansion process. The lower failure properties observed for composite samples could also be due to weak interfacial bonding at the graphite/matrix interface and the presence of aggregated graphite nanosheets. Further efforts will be made in the future to improve the interfacial bonding (through the surface functionalization of the graphite nanosheets) and the nanofiller dispersion degree (through the optimization of the processing parameters).

## Conclusions

PA11-based composites with two different kinds of graphite nanofillers (EG and NEG) at various concentrations were prepared through a melt compounding process and thermo-mechanically characterized. From XRD, SEM and BET, it was possible to conclude that the graphite expansion was successfully obtained. Moreover, XRD tests on the PA11/graphite composites indicated how the original crystal structure of the PA11 matrix was retained even after filler addition, while the presence of diffraction peaks associated to graphite indicated the presence of stacked lamellae within the composites. A slight improvement in the thermal stability of the material was detected for EG composites at elevated concentrations, while dynamical and quasi-static tensile tests highlighted how the stabilizing effect due to graphite addition was associated to a progressive embrittlement of the samples.


## Declaration of conflicting interests

The author(s) declared no potential conflicts of interest with respect to the research, authorship and/or publication of this article.

## Funding

The author(s) received no financial support for the research, authorship and/or publication of this article.

## ORCID iD

A Sola  <https://orcid.org/0000-0002-8649-9388>

## References

1. Laun S, Pasch H, Longi  ras N, et al. Molar mass analysis of polyamides-11 and -12 by size exclusion chromatography in HFIP. *Polymer (Guildf)* 2008; 49: 4502–4509.
2. Jacek Wesolowski KP. The polyamide market. *Fibres Text East Eur* 2016; 24: 12–18.
3. Romao W, Castro EVR, Filho EAS, et al. Ageing of polyamide 11 used in the manufacture of flexible piping. *J Appl Polym Sci* 2009; 114(3): 1777–1783.
4. Martino L, Basilissi L, Farina H, et al. Bio-based polyamide 11: synthesis, rheology and solid-state properties of star structures. *Eur Polym J* 2014; 59: 69–77.
5. Dorigato A, Brugnara M and Pegoretti A. Novel polyamide 12 based nanocomposites for industrial applications. *J Polym Res* 2017; 24: 96.
6. Andrea Dorigato LF. Thermo-mechanical behavior of polyamide 12—polyamide 66 recycled fiber composites. *Polym Compos* 2011; 32(5): 786–795.
7. Yang Z, Huang S and Liu T. Crystallization behavior of polyamide 11/multiwalled carbon nanotube composites. *J Appl Polym Sci* 2011; 122(1): 551–560.
8. Zhang Y, Wang B and Hu G. Isothermal crystallization kinetics and melting behavior of polyamide 11/silica nanocomposites prepared by in situ melt polymerization. *J Appl Polym Sci* 2012; 123(1): 273–279.
9. Li Y, Hu G and Wang B. Morphology development and non-isothermal crystallization behavior of polyamide 11/ethylene-vinyl alcohol blends. *J Appl Polym Sci* 2010; 118(4): 2126–2133.

10. Sahnoun M, Taguet A, Otazaghine B, et al. Inner surface modification of halloysite nanotubes and its influence on morphology and thermal properties of polystyrene/polyamide-11 blends. *Polym Int* 2017; 66: 300–312.
11. Jariyavidyanont K, Focke W and Androsch R. Crystallization kinetics of polyamide 11 in the presence of sepiolite and montmorillonite nanofillers. *Colloid Polym Sci* 2016; 294(8): 1143–1151.
12. Halim KAA, Farrell JB and Kennedy JE. Preparation and characterisation of polyamide 11/montmorillonite (MMT) nanocomposites for use in angioplasty balloon applications. *Mater Chem Phys* 2013; 143(1): 336–348.
13. Ferry L, Sonnier R, Lopez-Cuesta JM, et al. Thermal degradation and flammability of polyamide 11 filled with nanoboehmite. *J Therm Anal Calorim* 2017; 129: 1029–1037.
14. Dorigato A, D'Amato M and Pegoretti A. Thermo-mechanical properties of high density polyethylene-fumed silica nanocomposites: effect of filler surface area and treatment. *J Polym Res* 2012; 19: 1–11.
15. Yasmin A, Luo J and Daniel IM. Processing of expanded graphite reinforced polymer nanocomposites. *Compos Sci Technol* 2006; 66(9): 1179–1186.
16. Fukushima H and Drzal LT. Graphite nanoplatelets as reinforcements for polymers: structural and electrical properties. In: *17th technical conference American Society for Composite*, West Lafayette, US, 21–23 October 2002, pp. 1–9.
17. Fukushima K, Murariu M, Camino G, et al. Effect of expanded graphite/layered-silicate clay on thermal, mechanical and fire retardant properties of poly(lactic acid). *Polym Degrad Stab* 2010; 95(6): 1063–1076.
18. Camino G, Duquesne S, Delobel R, et al. Mechanism of expandable graphite fire retardant action in polyurethanes. In: Wilkie CA and Nelson GL (eds) *Fire and Polymers*. ACS Symposium Series. Washington, USA: ACS Pub, 2001, pp. 797.
19. Furdin G. Exfoliation process and elaboration of new carbonaceous materials. *Fuel* 1998; 77(6): 479–485.
20. Focke WW, Badenhorst H, Mhike W, et al. Characterization of commercial expandable graphite fire retardants. *Thermochim Acta* 2014; 584: 8–16.
21. Sorokina NE, Shornikova ON and Avdeev VV. Stability limits of graphite intercalation compounds in the systems graphite–HNO<sub>3</sub>–H<sub>2</sub>SO<sub>4</sub>–H<sub>2</sub>O–KMnO<sub>4</sub>. *Inorg Mater* 2007; 43(8): 822–826.
22. Chung DDL. Exfoliation of graphite. *J Mater Sci* 1987; 22(12): 4190–4198.
23. Fock WW, Muiambo H, Mhike W, et al. Flexible PVC flame retarded with expandable graphite. *Polym Degrad Stab* 2014; 100(1): 63–69.
24. Uhl FM, Yao Q, Nakajima H, et al. Expandable graphite/polyamide-6 nanocomposites. *Polym Degrad Stab* 2005; 89(1): 70–84.
25. Li Z and Qu B. Flammability characterization and synergistic effects of expandable graphite with magnesium hydroxide in halogen-free flame-retardant EVA blends. *Polym Degrad Stab* 2003; 81(3): 401–408.
26. Wei P, Bocchini S and Camino G. Flame retardant and thermal behavior of polylactide/expandable graphite composites. *Polimery* 2013; 5: 3–6.
27. Mhike W and Fock WW. Surface resistivity and mechanical properties of rotationally molded polyethylene/graphite composites. *J Vinyl Addit Technol* 2013; 19(4): 258–270.
28. Mago G, Kalyon DM and Fisher FT. Nanocomposites of polyamide-11 and carbon nanostructures: development of microstructure and ultimate properties following solution processing. *J Polym Sci B Polym Phys* 2011; 49(18): 1311–1321.

29. Demitri C, Moscatello A, Giuri A, et al. Preparation and characterization of EG-Chitosan nanocomposites via direct exfoliation: a green methodology. *Polymers (Basel)* 2015; 7(12): 2584–2594.
30. Mhike W, Ferreira IVW, Li J, et al. Flame retarding effect of graphite in rotationally molded polyethylene/graphite composites. *J Appl Polym Sci* 2015; 132: 1–11.
31. Focke WW, Kruger HJ, Mhike W, et al. Polyethylene flame retarded with expandable graphite and a novel intumescent additive. *J Appl Polym Sci* 2014; 40493: 1–8.
32. Liu T, Lim KP, Tjiu WC, et al. Preparation and characterization of nylon 11/organoclay nanocomposites. *Polymer (Guildf)* 2003; 44: 3529–3535.
33. Hocker S, Rhudy AK, Ginsburg G, et al. Polyamide hydrolysis accelerated by small weak organic acids. *Polymer (Guildf)* 2014; 55(20): 5057–5064.